Albumin-Binding and Tumor Vasculature Determine the Antitumor Effect of 15-Deoxy-Delta(12,14)-Prostaglandin-J(2) In Vivo

Prakash, Jai; Bansal, Ruchi; Post, Eduard; de Jager-Krikken, Alie; Lub-de Hooge, Marjolijn N.; Poelstra, Klaas

Published in:
Neoplasia

DOI:
10.1593/neo.91188

NEOPLASIA
www.neoplasia.com
Volume 11 Number 12 December 2009 pp. 1348–1358 1348

Albumin-Binding and Tumor Vasculature Determine the Antitumor Effect of 15-Deoxy-$\Delta^{12,14}$-Prostaglandin-J_2 *In Vivo*[1]

Jai Prakash*,†, Ruchi Bansal*, Eduard Post*, Alie de Jager-Krikken*, Marjolijn N. Lub-de Hooge‡ and Klaas Poelstra*,†

*Department of Pharmacokinetics, Toxicology and Targeting, Groningen Research Institute for Pharmacy, University of Groningen, Groningen, The Netherlands; †BiOrion Technologies BV, Groningen, The Netherlands; ‡Department of Nuclear Medicine and Molecular Imaging, University Medical Centre Groningen, Groningen, The Netherlands

Abstract

15-Deoxy-$\Delta^{12,14}$-prostaglandin-J_2 (15d-PGJ_2), a peroxisome proliferator–activated receptor γ (PPARγ) agonist, induces cell death in tumor cells *in vitro*; however, no study showed its *in vivo* effect on tumors. Here, we report that 15d-PGJ_2 shows antitumor effects *in vivo* in mice. However, its effects correlate with tumor uptake of albumin, to which it reversibly binds. 15d-PGJ_2 induces cell death in B16F10 melanoma and C26 colon carcinoma cells *in vitro*. These effects were not elicited through PPARγ-dependent pathways because an irreversible PPARγ antagonist GW9662 did not inhibit these effects. Caspase- and nuclear factor κB– (NF-κB) dependent pathways were found to be involved as determined with caspase-3/7 fluorescent assay and NF-κB containing plasmid transfection assay, respectively. Noticeably, 15d-PGJ_2 had significantly stronger effects in C26 cells compared with B16 cells in all assays. However, *in vivo*, there was no effect on C26 tumors, yet it significantly inhibited the B16 tumor growth in mice by 75%. We found that 15d-PGJ_2 rapidly bound to albumin and *in vivo* albumin greatly distributed to B16 tumors compared with C26 tumors, shown with γ-camera imaging and immunohistochemical staining. Albumin accumulation can be attributed to the large blood vessel diameter in B16 tumors and an enhanced permeability and retention effect. These findings suggest that 15d-PGJ_2 can be an effective therapeutic agent for cancer, although its effects seem to be limited to the tumors allowing albumin penetration.

Neoplasia (2009) 11, 1348–1358

Introduction

Prostaglandins are the hormone-like lipids produced locally by a variety of cells in response of external stimuli. They play a crucial role in the regulation of smooth muscle tone, homeostasis, inflammation, cellular growth, and differentiation [1]. Among all prostaglandins, 15-deoxy-$\Delta^{12,14}$-prostaglandin J_2 (15d-PGJ_2), a metabolite of PGD_2, has a unique property to activate the nuclear receptor peroxisome proliferator–activated receptor γ (PPARγ) [2]. 15d-PGJ_2 is a highly interesting prostaglandin because it possesses multiple pharmacological activities, such as anti-inflammatory, antifibrotic, and apoptotic activities [3–7]. However, it has been shown that intracellular levels of 15d-PGJ_2 (pM range) are far below the concentrations (2.5-100 μM) required to exert its pharmacological effects [8]. Considering the potent biologic effects of 15d-PGJ_2 *in vitro* and its *in vivo* effect on key processes of inflammation, regeneration and tissue growth, exogenous administration of 15d-PGJ_2 may be quite relevant but insight in factors that control its local effectiveness is warranted. This is true for many prostaglandins, but in particular, the potential applications of 15d-PGJ_2 are quite unclear. Although 15d-PGJ_2 has

Abbreviations: 15d-PGJ_2, 15-deoxy-$\Delta^{12,14}$-prostaglandin-J_2; B16, B16F10 melanoma cells; PPARγ, peroxisome proliferator–activated receptor-γ; NF-κB, nuclear factor κB; HSA, human serum albumin; PBS, phosphate-buffered saline

Address all correspondence to: Dr. Jai Prakash, PhD, Department of Pharmacokinetics, Toxicology and Targeting, Groningen Research Institute for Pharmacy, University of Groningen, Antonius Deusinglaan 1, 9713 AV, Groningen, the Netherlands.
E-mail: J.Prakash@rug.nl

[1]This study was supported by STW Valorisation Grant, the Netherlands.
Received 15 July 2009; Revised 11 September 2009; Accepted 14 September 2009

DOI 10.1593/neo.91188

been found to elicit its pharmacological effects through PPARγ-dependent pathway, several studies have also shown that it can act through many PPARγ-independent pathways such as nuclear factor κB (NF-κB)–, Keap-Nrf2–, and p53-dependent pathways [7,9,10].

In literature, 15d-PGJ_2 has been shown to induce apoptosis-mediated cell death in a variety of tumor cells *in vitro* [11–15]. However, there are nearly no data showing beneficial effects of 15d-PGJ_2 in tumor models *in vivo*. Fulzele et al. [16] demonstrated that treatment with 15d-PGJ_2 enhanced the antitumor effects of docetaxel in animal tumor models, but 15d-PGJ_2 did not show any inhibitory effects by itself. The reason for the ineffectiveness of 15d-PGJ_2 *in vivo* might be due to the loss of its biologic activity in the presence of serum as demonstrated in cell culture systems [17,18]. Conversely, many studies have shown the *in vivo* therapeutic effects of 15d-PGJ_2 in inflammatory diseases such as acute pancreatitis [19] and ischemia-reperfusion injuries in heart, brain, kidneys, and gut [20–24]. Therefore, it can be assumed that 15d-PGJ_2 remains pharmacologically active *in vivo* after systemic administration. However, there might be some factors that regulate the efficacy of 15d-PGJ_2 *in vivo*.

In the present study, we investigated the effects of 15d-PGJ_2 in two different tumor cell types, that is, B16F10 melanoma and C26 colon carcinoma *in vitro* and furthermore investigated its mechanism of action in these cells. In addition, we compared its *in vivo* efficacy in the subcutaneously induced tumors from these cells in mice. We found that the *in vivo* effectiveness of 15d-PGJ_2 did not correlate with our *in vitro* results. To that end, we explored the following in more detail: 1) interaction of 15d-PGJ_2 with the serum protein albumin, 2) distribution of albumin in both tumor types, and 3) effect of tumor vascularization on the albumin uptake in these tumors to determine the reason for the difference between *in vitro* and *in vivo* efficacy of 15d-PGJ_2.

Materials and Methods

Materials

Mouse colon carcinoma cells (C26) were kindly provided by Prof. Molema (Medical Biology, University Medical Centre Groningen, the Netherlands) and mouse melanoma cells (B16F10) were bought from American Type Culture Collection (ATCC, Rockville, MD). Monoclonal rat-antimouse platelet endothelial cell adhesion molecule-1 (CD31) was purchased from BD PharMingen (San Diego, CA), and was purchased from rabbit–anti–human serum albumin (HSA) from ICN Biomedics (Eschwege, Germany). Human serum albumin (HSA; GMP-grade Cealb) was purchased from Sanquin (Amsterdam, Netherlands), and mouse serum albumin (fraction V) was bought from Sigma (St Louis, MO). Mouse tumor necrotic factor α (TNF-α) was bought from Peprotech (Rocky Hill, NJ). GW9662 (2 chloro 5-nitrobenzanilide) was purchased from Sigma.

Immunohistochemistry and Immunocytochemistry

From isopentane-fixed tissues, 4-μm-thick frozen sections were made with a cryostat (Leica, Nussloch, Germany) to perform immunohistochemical staining. Sections were fixed in acetone for 20 minutes, and cells were fixed in acetone-methanol (1:1) at –20°C for 1 hour. Sections or cells were dried under blowing air, rehydrated in phosphate-buffered saline (PBS), and then incubated with primary antibody of interest for 1 hour. After three washings with PBS, endogenous peroxidase activity was blocked with 0.05% hydrogen peroxide by incubating for 20 minutes only in case of tissue sections. Then, sections/cells were incubated with horseradish peroxidase–labeled secondary antibody for 30 minutes after three washings with PBS. Then, samples were washed three times with PBS and incubated with 3-amino-9-ethyl carbazole solution for 20 minutes. Subsequently, samples were washed in distilled water and incubated with hematoxylin for nuclear staining. After this, tissue sections or cells were mounted with glycerol/kieselguhr solution after washing in tap water. Staining was visualized under a light microscope (Olympus BX41, Tokyo, Japan).

We analyzed CD31 staining (endothelial cell marker) for the determination of the blood vessel lumen area and blood vessel density in tumor sections of B16 and C26 tumors using NIH Image software (Image J; National Institutes of Health, Bethesda, MD). To measure blood vessel lumen area, we randomly selected approximately 40 blood vessels of B16 tumor and 100 blood vessels of C26 tumor per animal in three mice and drew a line around the CD31 staining digitally and measured the area of the drawn circle with the software. For measuring the blood vessel density, we counted the number of blood vessels in three to four different tumor fields per animal at the magnification of ×100 in $n = 3$ mice for each tumor.

Cell Experiments

B16 and C26 cells were maintained on Dulbecco's modified Eagle's medium (BioWhittaker, Verviers, Belgium) supplemented with 10% fetal calf serum (FCS) and antibiotics (50 U/ml penicillin plus 50 ng/ml streptomycin for B16 and 10 μg/ml gentamicin for C26 cells) at 37°C in a humidified incubator containing 5% carbon dioxide.

Cell growth determination. Cells were seeded into the 96-well plate as 1×10^4 cells/well in 200 μl medium with 10% FCS. After 24 hours, cells were washed with serum-free medium and then incubated with different concentrations of 15d-PGJ_2 in serum-free medium for 48 hours. In case of treatment with GW9662, cells were preincubated with GW9662 (10 μM) for 3 hours and then incubated with a mixture of 15d-PGJ_2 and GW9662 for 48 hours. For other treatments such as FCS and HSA, cells were incubated with 15d-PGJ_2 simultaneously. Cell growth was determined using alamarBlue dye (Serotec, Oxford, UK), which reflects the number of cells on the basis of mitochondrial activity. After 48 hours of incubation, cells were added with the medium containing the alamarBlue Dye (diluted 1:10) and incubated for 4 hours, and thereafter, the metabolized dye (fluorescent) was detected with a fluorimeter at an excitation of 560 nm and an emission of 590 nm.

Caspase 3/7 enzyme assays. Caspase-3 and -7 enzymes activity was determined using Caspase 3/7 Glo Assay Kit (Promega, Madison, WI). A total of 1×10^4 cells were seeded in 96-well plate in 200 μl of culturing medium. After 24 hours, cells were washed with serum-free medium and incubated with different concentrations of 15d-PGJ_2 in a 100-μl medium for 5.5 hours. Subsequently, 100 μl of the caspase 3/7 reconstituted reagent was added to the cells and incubated for 30 minutes in the incubator. The luminescence was determined by a luminometer (Lumicount; Packard, Meriden, CT).

Transfection and luciferase assay for NF-κB activity. The activity of NF-κB was determined with a Luciferase assay using a Luciferase plasmid DNA, pNF-κB-Luc (Clontech, Mountain View, CA), which contains a specific binding sequence for NF-κB. An empty Luciferase

plasmid, pTAL-Luc was used as a control. In brief, 1×10^4 cells per well were seeded in 96-well plates, and the transfection of the plasmid was carried out using FuGENE 6 Transfection Reagent (Roche, Mannheim, Germany) after 24 hours. Cells were treated with a complex of 0.17 μg of DNA/0.5 μl of FuGENE 6 in 100 μl of normal medium with 10% FCS for 24 hours. Subsequently, cells were washed once with serum-free medium and incubated with 15d-PGJ_2 with or without TNF-α for 4 hours. Thereafter, cells were washed with PBS and lysed with 20 μl of lysis buffer and added with 100 μl of Luciferase substrate (Promega). Luciferase activity was measured by a luminometer (Lumicount; Packard). The luminescence unit values of pNF-κB-Luc were neutralized by subtracting the pTAL-Luc values.

Binding Studies of 15d-PGJ_2 to Albumin

To determine the binding of 15d-PGJ_2 with HSA and mouse albumin, 15d-PGJ_2 (10 μM dissolved in PBS) was incubated with HSA (30 and 80 μM in PBS) and mouse albumin (30 μM) for 15 minutes and 3 hours at 37°C. At specific time points, samples were taken out and put into the centrifuge dialysis tubes (Microcon, cutoff 10 kDa; Millipore, Bedford, MA) and centrifuged for 20 minutes at ×14,000 rpm to separate unbound 15d-PGJ_2. The filtrate from the centrifuge tube was collected, and 25 μl of it was injected into an HPLC system (Waters, Milford, MA) to quantify 15d-PGJ_2. Control tubes with 10 μM 15d-PGJ_2 alone were included and processed in the similar way to examine the percentage recovery from the centrifuge dialysis tubes. HPLC determination of 15d-PGJ_2 was performed with Chromolith SpeedROD column (Merck, Darmstadt, Germany) with eluents (acetonitrile/H_2O/trifluoroacetic acid, 50:50:0.1) at a flow rate of 1 ml/min. 15d-PGJ_2 was detected using a UV detector at 306 nm and quantified using EmPower software (Waters).

To investigate whether 15d-PGJ_2 was covalently bound to albumin, we used fast protein liquid chromatography system (FPLC, AKTA; Amersham Biosciences, Uppsala, Sweden). 15d-PGJ_2 (10 μM) was incubated with HSA (80 μM) overnight at 37°C. Thereafter, the mixture was injected into a FPLC system equipped with gel filtration column (Superdex 200; Amersham Biosciences) and UV detector (214 nm).

Subcutaneous Tumor Model in Mice

Normal male C57BL/6 and Balb/c mice weighing 20 to 25 g were obtained from Harlan (Zeist, the Netherlands). They were kept at a 12:12-hour light/dark cycle and received *ad libitum* normal diet. All experimental protocols for animal studies were approved by the Animal Ethics Committee of the University of Groningen. To induce subcutaneous tumors, B16F10 cells and C26 cells were cultured in 125-mm^3 flasks a day before injection in animals to keep them in the growth phase. Cells were detached by trypsanization, and trypsin was

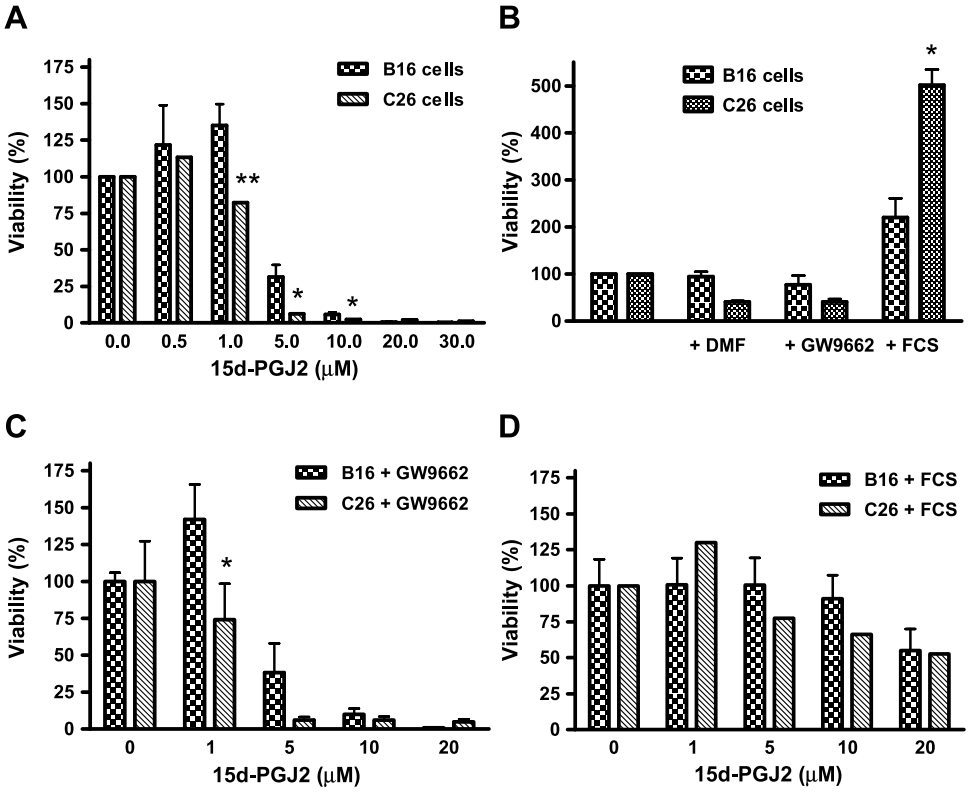

Figure 1. Effect of 15d-PGJ_2 on the growth of B16 and C26 cells. (A) 15d-PGJ_2 induced cell death in both B16 and C26 tumor cells. However, the effects were significantly higher in C26 cells compared with B16 cells. (B) Incubation of control cells with the PPARγ antagonist GW9662 (10 μM) and 5% FCS affected the cell growth of both cell types. (C) Pretreatment with GW9662 did not inhibit the effect of 15d-PGJ_2 in both cell types indicating the PPARγ-independent effects of 15d-PGJ_2. (D) Incubation of 15d-PGJ_2 in the presence of FCS reduced its effects in both cell types. Data are presented as relative fluorescence unit that was calculated by fixing the intensity of fluorescent product of alamarBlue dye for untreated cells at 100. Data represent the average of at least three separate experiments. Statistical differences between B16 and C26 cells are shown as $^*P < .05$, $^{**}P < .01$.

removed by centrifugation. The cell pellet was resuspended in PBS. A total of 1×10^6 cells (B16 and C26 cells) suspended in 100 μl of PBS were injected subcutaneously in the flank of C57BL/6 and Balb/c mice, respectively. Tumor growth was followed by measuring tumor size using a digital Vernier caliper. Tumor volume was established using the formula: $a \times b^2 / 2$, where a denotes tumor length and b denotes the tumor width.

Effect of 15d-PGJ$_2$ on tumor growth. B16 and C26 tumors were induced in mice as described previously. The treatment was started on day 5 when the tumor volume was reached the range of 50 to 100 mm^3 because this tumor size has been shown as an optimum tumor size for the start of the treatment [25,26]. Animals were injected intravenously with four doses of either vehicle (PBS) or 15d-PGJ$_2$ (2 mg/kg per day) on alternative days under anesthesia (O_2/isoflurane). Tumor size was measured under anesthesia. Animals with B16 tumors were killed on day 13 as the tumor volume in some animals reached to 2000 mm^3 (maximally allowed by the ethical guidelines), whereas the animals with C26 tumors were killed on day 15 because no effect of the treatment was observed. Animals were killed under gas anesthesia (O_2/isoflurane), and tumors were isolated and fixed in cold isopentane for cryosections.

γ-Camera imaging of ^{123}I-HSA and tumor distribution of HSA. HSA was radiolabeled with radioiodine (^{123}I) using NBS method on the same day of the experiment as explained elsewhere [27]. The tracer doses (3-4 MBq) of ^{123}I-labeled HSA were injected intravenously into tumor-bearing mice through penile vein under anesthesia (O_2/isoflurane). Two hours after injection, animals were scanned with a γ-camera for 10 minutes under ketamine/diazepam anesthesia. Subsequently, the same animals were rescanned at t = 24 hours. The experiments were performed in three animals per time point for each tumor type.

To localize HSA in both B16 and C26 tumors, HSA (1 mg per mouse) was injected intravenously into the tumor-bearing mice. After 2 hours, animals were killed, and tumors were isolated and fixed in cold isopentane. Tumor tissues were processed for immunohistochemical analyses using anti-HSA antibody as described previously.

Statistical Analyses

Data are presented as mean ± SEM unless otherwise mentioned. The statistical analyses were performed using Student's t-test with $P < .05$ as the minimal level of significance. AlamarBlue data were fitted for sigmoidal dose-response curve to calculate the half maximal inhibitory concentration (IC_{50}) using GraphPad Prism 4 software (La Jolla, CA).

Results

15d-PGJ$_2$ Induces Cell Death in B16 and C26 Cells PPARγ-Independently

Treatment with 15d-PGJ$_2$ caused cell death in both B16 and C26 cells in a dose-dependent manner (Figure 1*A*). 15d-PGJ$_2$ showed a significantly higher efficacy in C26 cells (IC_{50} = 1.52 μM) compared with the B16 cells (IC_{50} = 4.52 μM). Although 15d-PGJ$_2$ is known to induce its effects through the PPARγ pathway, we found that cell death in these cells was PPARγ-independent because pretreatment with the irreversible PPARγ antagonist GW9662 did not block the effects of 15d-PGJ$_2$ (Figure 1*C*). Also, in the presence of GW9662, C26 cells were found to be more sensitive than B16 cells for the treatment with 15d-PGJ$_2$. Furthermore, we found that the presence of serum substantially reduced the growth-inhibiting effect of 15d-PGJ$_2$ in both cell types (Figure 1*D*). The inhibition of this effect might be due to the binding of 15d-PGJ$_2$ to the serum proteins [17]. These data suggest that *in vivo*, 15d-PGJ$_2$ might become ineffective owing to the presence of a large amount of serum proteins in circulation.

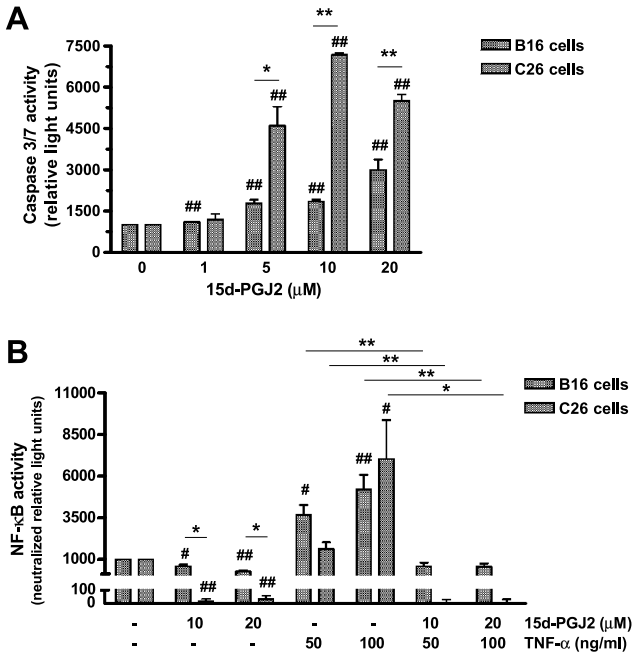

Figure 2. Effect of 15d-PGJ$_2$ on the caspase 3/7 activity and NF-κB activity in B16 and C26 cells. (A) Caspase 3/7 enzyme activity was determined in cells using a luminescence assay after the incubation with different amount of 15d-PGJ$_2$ for 5.5 hours as described in the Materials and Methods section. Data show that the caspase 3/7 activity was induced in both cell types by 15d-PGJ$_2$ concentration-dependently. However, C26 cells had significantly higher activity than B16 cells. (B) For NF-κB activity, both B16 and C26 cells were transiently transfected with a plasmid containing NF-κB promoter with luciferase reporter element (pNF-κB-Luc) for 24 hours. In parallel, an empty plasmid with only luciferase activity (pTAL-Luc) was used as a control. After 24 hours, 15d-PGJ$_2$ was incubated with and without TNF-α for 4 hours, and then luciferase activity was measured using luminescence assay to determine the NF-κB activity. The values (relative light units) of the pNF-κB-Luc were neutralized by subtracting the values of the control plasmid pTAL-Luc. The NF-κB pathway activator, TNF-α, induced the NF-κB activity in both cell types and treatment with 15d-PGJ$_2$ significantly inhibited it. In control cells, inhibitory effects of 15d-PGJ$_2$ were more pronounced in C26 cells. Data represent for the average of at least three separate experiments. Statistical differences *versus* the respective controls are shown as $^{\#}P < .05$ and $^{\#\#}P < .01$ and other differences are $^{*}P < .05$, $^{**}P < .01$.

15d-PGJ$_2$ Induces Apoptosis by Inhibiting NF-κB Pathway

To confirm that 15d-PGJ$_2$ caused cell death in B16 and C26 cells through apoptotic pathways, we determined the activities of caspase-3

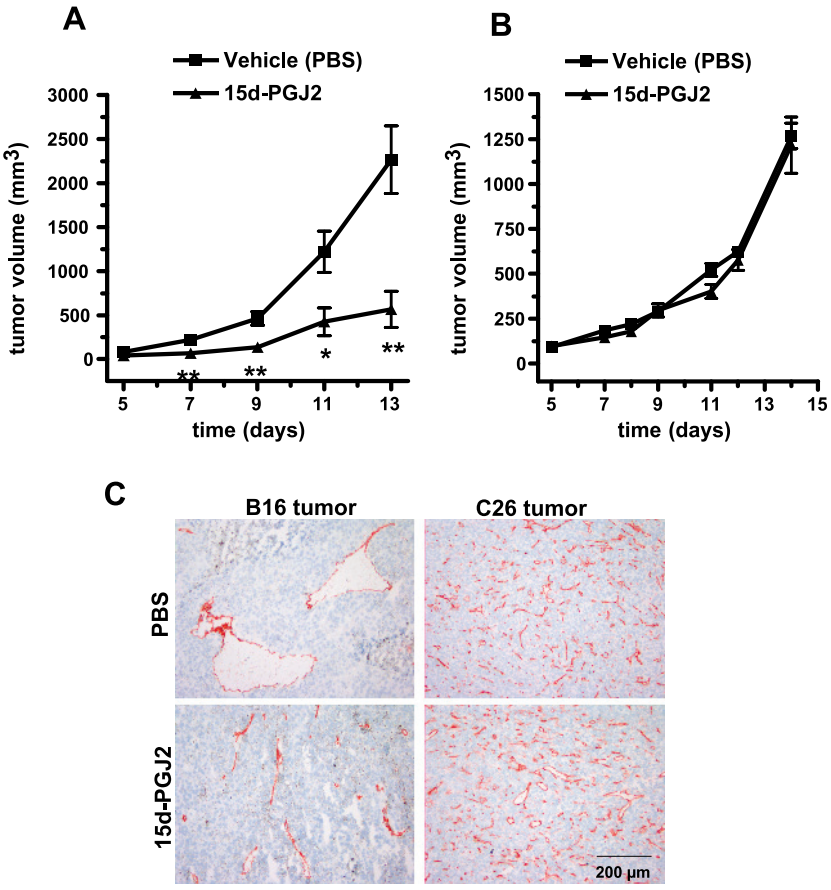

Figure 3. *In vivo* effects of 15d-PGJ_2 on the tumor growth B16 and C26 tumors. B16 and C26 tumor-bearing mice were treated either with PBS or 15d-PGJ_2 (2 mg/kg per day) intravenously. Treatment with 15d-PGJ_2 significantly (*$P < .05$, **$P < .01$ *vs* vehicle group) retarded the progression of B16 tumors (A), whereas no effect found on the growth of C26 tumors (B). Data represent the average of six animals per group for all groups. (C) Representative microscopic pictures of the endothelial cell marker CD31 staining showing the effect of 15d-PGJ_2 on the vasculature of B16 and C26 tumors. Treatment with 15d-PGJ_2 disrupted the blood vessels in B16 tumors, whereas there was no effect on the vasculature of C26 tumors.

and -7, the effector enzymes in apoptosis pathway. We found that 15d-PGJ_2 caused a concentration-dependent increase in caspase-3 and -7 enzymes activity in both cell types after 6 hours of incubation. Again, the activity was significantly higher in C26 cells than in B16 cells (Figure 2*A*). These data suggest that C26 cells respond to 15d-PGJ_2 more promptly than B16 cells through activation of the apoptosis cascade.

Because the cell death induced by 15d-PGJ_2 was PPARγ-independent, we investigated the involvement of NF-κB pathway, an important regulator of cell apoptosis and proliferation, in B16 and C26 cells using the NF-κB luciferase reporter assay. To induce the NF-κB activity in these cells, we used TNF-α, which is a direct activator of NF-κB pathway. We found that treatment with TNF-α (50 and 100 ng/ml) significantly enhanced the NF-κB reporter activity (B16 cells, 3.7- and 5.2-fold, respectively, and C26 cells, 1.6- and 7.0-fold, respectively), which was in turn completely inhibited by 15d-PGJ_2 (Figure 2*B*). In addition, 15d-PGJ_2 also reduced the NF-κB activity in TNF-α–untreated cells. Similar to the studies mentioned previously, the effect was greater in C26 than in B16 cells. These results demonstrate that 15d-PGJ_2 induces apoptosis in both B16 and

Table 1. Plasma Levels of ALT, AST, and Creatinine in Tumor-Bearing Mice to Determine the Effect of the 15d-PGJ_2 Treatment on Liver and Renal Toxicity.

Tumor Models	Treatment Groups	ALT (U/L)	AST (U/L)	AST/ALT Ratio	Creatinine (μM)
B16 tumor-bearing mice	PBS (n = 5)	44.4 ± 7.2	602 ± 60.2	14.5 ± 2.0	7.80 ± 0.97
	15d-PGJ_2	35.2 ± 2.0	135 ± 20.1*	3.92 ± 0.6*	7.83 ± 1.0
C26 tumor-bearing mice	PBS	18.8 ± 1.4	67.8 ± 6.5	3.73 ± 0.5	8.0 ± 1.2
	15d-PGJ_2	14.5 ± 1.7†	56.2 ± 6.4	4.14 ± 0.8	9.67 ± 1.4

ALT indicates alanine aminotransferase; *AST*, aspartate aminotransferase.
n = 6 animals per group unless mentioned.
*$P < .01$, PBS *versus* 15d-PGJ_2.
†$P < .05$, PBS *versus* 15d-PGJ_2.

C26 cells through common pathways involving caspase- and NF-κB–dependent pathways.

15d-PGJ$_2$ Reduces the Tumor Progression In Vivo

Because 15d-PGJ$_2$ showed high cytotoxicity *in vitro* in both B16 and C26 cells, we further evaluated its efficacy *in vivo* in subcutaneous tumor-bearing mice from these cells. In B16 tumors, we found that treatment with 15d-PGJ$_2$ significantly inhibited the progression of tumors as shown in Figure 3 (*A* and *B*). These effects were visible from the first dose of 15d-PGJ$_2$, indicating a high efficacy of the treatment. 15d-PGJ$_2$–treated tumors had 80% lower tumor weight compared with the vehicle-treated tumors (0.30 ± 0.13 *vs* 1.67 ± 0.37 g, respectively, $P < .01$), and large necrotic area and disrupted vasculature could be seen after CD31 immunostaining (Figure 3*C*). Surprisingly, similar doses of 15d-PGJ$_2$ had no effect on the tumor growth of C26 tumors, although *in vitro* the C26 cells were more prone to the 15d-PGJ$_2$ treatment compared with the B16 cells. Treatment with 15d-PGJ$_2$ significantly reduced the raised alanine aminotransferase/aspartate aminotransferase levels in B16 tumor-bearing mice (Table 1). These data show that 15d-PGJ$_2$ did not cause any liver and renal toxicity in both tumor models (Table 1).

We set out to find the reason for this discrepancy in effectiveness of 15d-PGJ$_2$ *in vitro* and *in vivo* in both tumor models.

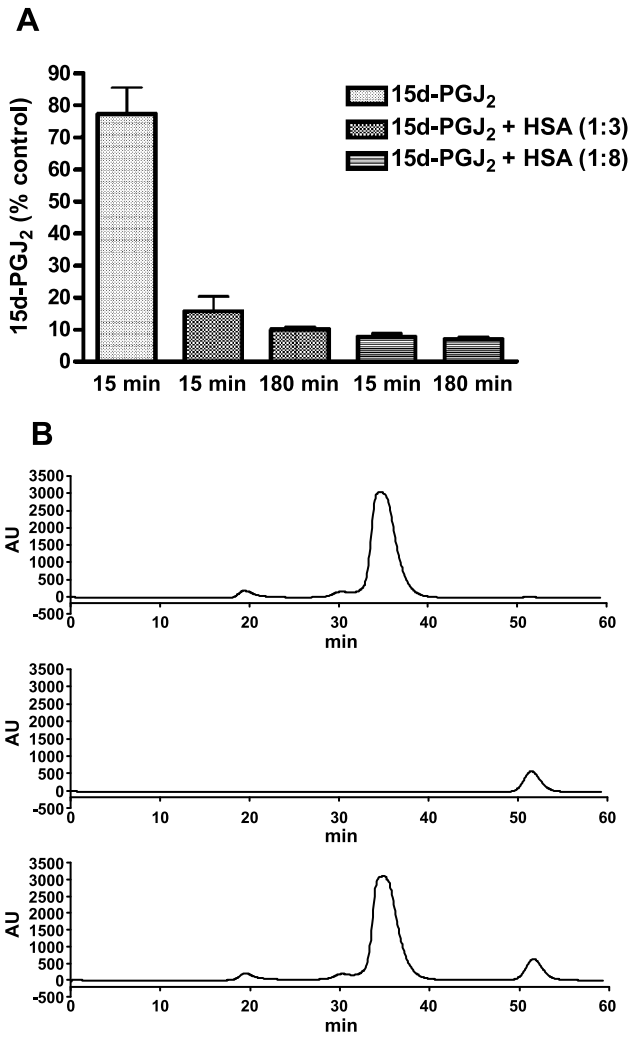

Figure 4. *In vitro* binding of 15d-PGJ$_2$ to albumin. (A) 15d-PGJ$_2$ (10 μM) rapidly bound to HSA (30 and 80 μM) within 15 minutes, and there was a slight increase in the binding after 3 hours. 15d-PGJ$_2$ and HSA were incubated at 37°C and 100-μl samples were withdrawn after 15 minutes and 3 hours. Then the samples were passed through the ultrafiltration units, and the filtrates were determined for 15d-PGJ$_2$ using the HPLC method. Data represent the percentage of the concentration of 15d-PGJ$_2$ in the incubation solution, and the experiments were done in triplicate. (B) Representative chromatogram of the size-exclusion chromatography performed on 15d-PGJ$_2$, HSA, and the mixture of 15d-PGJ$_2$ and HSA (1:8) after their incubation overnight at 37°C.

Binding of 15d-PGJ$_2$ to Albumin Determines Its Pharmacological Activity

We already showed that 15d-PGJ$_2$ lost its effects in the presence of serum *in vitro* (Figure 1*D*), and this could be the most likely cause of its ineffectiveness *in vivo*. However, 15d-PGJ$_2$ showed its anti–tumor effects in B16 tumors but not in C26 tumors, which indicates that there are more factors responsible for this discrepancy in effectiveness. Because albumin is the major protein in serum and has been shown to block the effects of 15d-PGJ$_2$ *in vitro* [17], we examined the binding of HSA to 15d-PGJ$_2$. We found that 85% of 15d-PGJ$_2$ was bound to HSA after a short incubation with three-fold molar excess of HSA at 37°C, as determined by HPLC analysis after separating the unbound 15d-PGJ$_2$ using an ultrafiltration method (Figure 4*A*). A higher molar ratio of HSA (eight-fold) enhanced the binding up to 90%. Because the *in vivo* effect studies were performed in mice, we investigated binding of 15d-PGJ$_2$ to mouse serum albumin. We found that 15d-PGJ$_2$ was completely bound to the mouse albumin (three-fold molar excess) within 15 minutes of incubation. In our *in vivo* study, the molar ratio of 15d-PGJ$_2$ to albumin is estimated to be 1:7.5, which means that no 15d-PGJ$_2$ was left unbound. This binding of 15d-PGJ$_2$ to albumin appeared to be noncovalent and reversible because 15d-PGJ$_2$ could be completely separated again from HSA after an overnight incubation at 37°C in 1:8 (15d-PGJ$_2$/HSA) ratio, when the mixture was passed through a gel filtration column in an FPLC system (Figure 4*B*). Similar results were obtained when the mouse albumin–15d-PGJ$_2$ complex was put on gel filtration column (data not shown), indicating the reversibility of the 15d-PGJ$_2$ binding to albumin.

Subsequently, we examined whether HSA interferes in the activity of 15d-PGJ$_2$ *in vitro* in both cell types. We found that HSA reduced the 15d-PGJ$_2$ caused cell death in both B16 and C26 cells, although the blockade was more pronounced in B16 cells (Figure 5). A 2.5-fold molar excess of HSA was sufficient to block the effect of 15d-PGJ$_2$ (10 μM) by 90% in B16 cells, but in C26 cells, the effects were not blocked for more than 40% even with five-fold excess of HSA (Figure 5, *C* and *D*). Because, in both cases, HSA binds to 15d-PGJ$_2$, we tested whether C26 cells might be able to internalize HSA–15d-PGJ$_2$ complex and release active 15d-PGJ$_2$ intracellularly. We therefore incubated B16 and C26 cells with HSA (30 μM) and HSA (30 μM) plus 15d-PGJ$_2$ (10 μM) for 24 hours and performed anti-HSA staining after removing unbound protein by washing several times. We found that C26 cells displayed significant staining for HSA, whereas B16 cells showed no staining at all. These results indicate that the 15d-PGJ$_2$–HSA complex formed in the medium can enter C26 cells. This may cause release of active 15d-PGJ$_2$ leading to the observed effects in this cell type. B16 cells do not take up this complex *in vitro*.

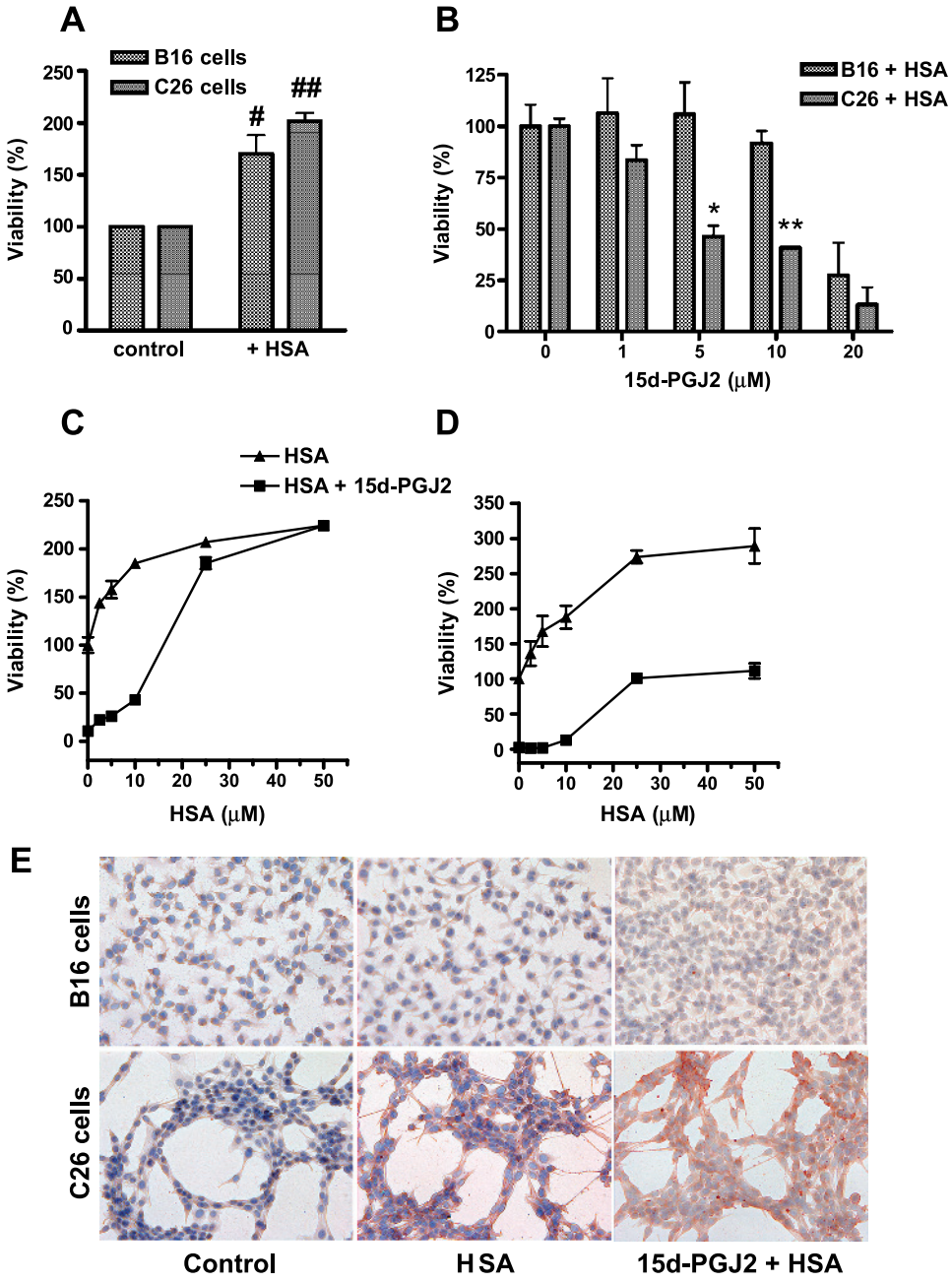

Figure 5. Effect of HSA on the effects of 15d-PGJ_2 in both B16 and C26 cells. (A) Incubation of HSA in both cell types enhanced their growth compared with the control cells in serum-free medium. $^{\#}P < .05$ and $^{\#\#}P < .01$ show the differences *versus* the respective controls. (B) Addition of HSA (30 μM) reduced the activity of 15d-PGJ_2 in both cell types after 48 hours; however, these inhibitory effects were significantly higher in B16 cells compared with C26 cells. Data represent the average of three experiments, and $^{*}P < .05$ and $^{**}P < .01$ show the differences between B16 and C26 cells. (C) 15d-PGJ_2 (10 μM) killed both tumor cell types almost completely, and the addition of HSA blocked its activity with the increasing amounts. (D) However, in C26 cells, the growth did not reach to the maximal level with the highest concentration of HSA. (E) Representative microscopic pictures of anti-HSA immunostaining in B16 and C26 cells. A total of 4×10^4 cells/well were grown in 24-well plates and incubated with HSA (30 μM) and HSA (30 μM) plus 15d-PGJ_2 (10 μM) for 24 hours and then washed three times with PBS, and anti-HSA immunostaining was performed. Red color showed the positive staining for HSA in C26 cells, whereas there was no staining in B16 cells.

Differences in the Tumor Vasculature Permits/Rejects Albumin Tumor Uptake and Thereby May Influence the Effect of 15d-PGJ_2

From the mentioned results, we conclude that 15d-PGJ_2 can bind to albumin in a reversible manner immediately after intravenous injection, and this profoundly attenuates the biologic effects of 15d-PGJ_2. *In vitro*, B16 tumor cells are less sensitive to 15d-PGJ_2 and are more affected by this inhibitory effect of albumin compared with C26 tumors, yet *in vivo* the antitumor effect of 15d-PGJ_2 is much stronger in B16 tumors. Therefore, we assumed that tumor accessibility of albumin might explain the differences in the effects of 15d-PGJ_2 *in vivo*. Because tumor penetration of albumin may depend on the tumor vasculature, we determined the blood vessel lumen size and blood vessel density in both B16 and C26 tumors of different

sizes using CD31 immunostaining (an endothelial cell marker). We found that blood vessel lumen size was increased with the size of tumors in both tumor types (Figure 6, *A–F*). Interestingly, in B16 tumors, the blood vessel lumen area was eight times larger than C26 tumors, but the number of blood vessel per field was 7.5-fold higher in C26 tumors than in B16 tumors as quantified in tumors of similar size (Figure 6, *G* and *H*). This shows that both tumor types have a different vasculature. To determine whether tumor vasculature induces a difference in the HSA uptake, we examined the uptake of ^{123}I-HSA in B16 and C26 tumors using γ-camera imaging techniques. Interestingly, B16 tumors had a high distribution and uptake of HSA because tumors were clearly visible in the flank of the mice 2 and 24 hours after ^{123}I-HSA injection (Figure 7*A*). In contrast, C26 tumors were not visible at any time point, suggesting the poor distribution of ^{123}I-HSA to these tumors (Figure 7*A*). To confirm the results, we examined the distribution of HSA in the tumor-bearing

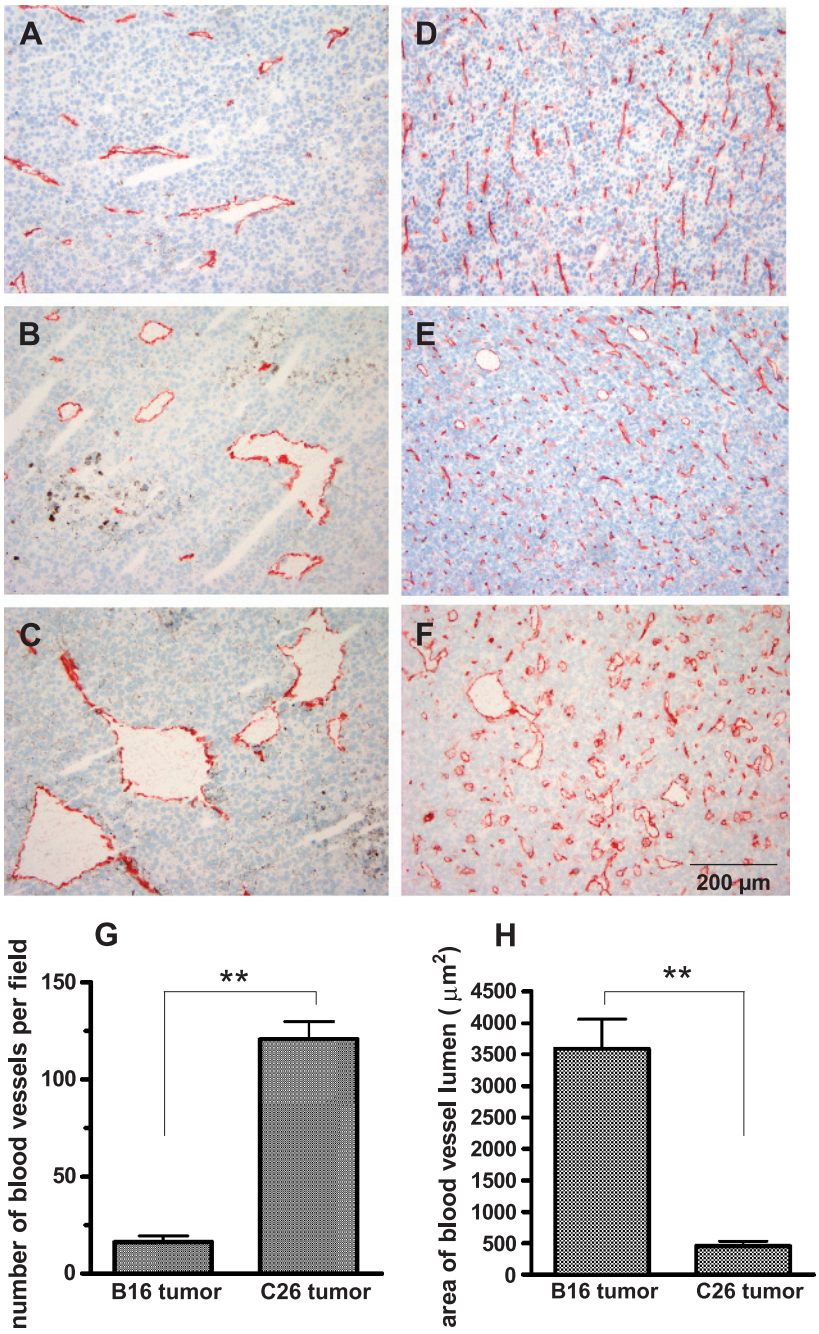

Figure 6. Representative microscopic pictures of anti-CD31 immunostaining (endothelial cell marker) in B16 and C26 tumors. Pictures show the difference in the tumor vasculature of B16 tumors (A, B, C) and C26 tumors (D, E, F) at their different sizes (A, D = 300-400 mm^3; B, E = 1300-1400 mm^3; C, F = ~2000 mm^3). The blood vessel lumen was found to be increased with the increase in the tumor size in both tumor types. (G) Quantitative data for the blood vessel density (number of blood vessels per field) showed that C26 tumors have significantly higher number of blood vessels than B16 tumors. In contrast, B16 tumors had significantly larger lumen area of the blood vessels than C26 tumors (H). These analyses were performed in B16 tumors (1616 ± 142 mm^3) and in C26 tumors (1593 ± 233 mm^3) from n = 3 mice for each tumor type. $^{**}P < .01$.

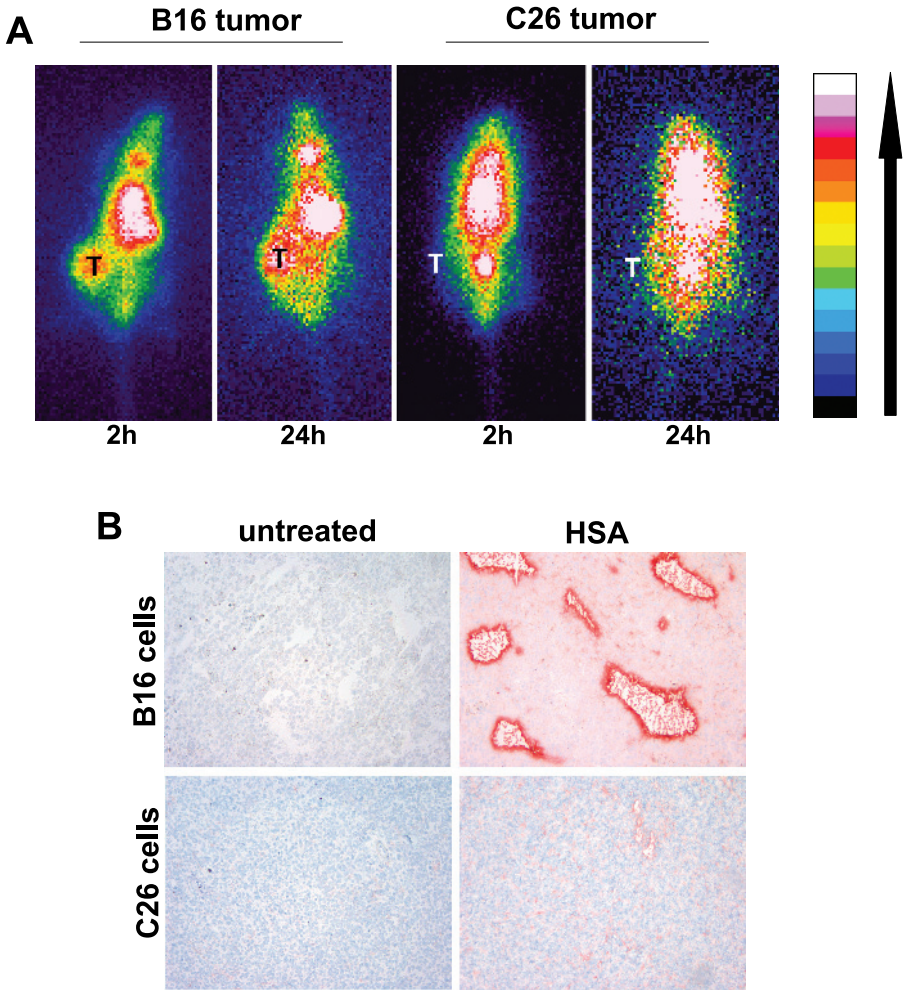

Figure 7. Tumor distribution of HSA in tumor-bearing mice. (A) Representative γ-camera images showing the whole-body scans of the tumor-bearing mice with B16 and C26 tumors at $t = 2$ hours and $t = 24$ hours after intravenous injection of the tracer doses of ^{123}I-HSA. Data demonstrate that ^{123}I-HSA was rapidly distributed to the B16 tumors within 2 hours but not to the C26 tumors. Each picture is representative of $n = 2$ to 3 mice. "T" denotes to the location of tumor in the flank of mice. Right multicolor bar indicates increase of the radioactivity. (B) Representative microscopic pictures of the anti-HSA immunostaining in B16 and C26 tumors. Tumor-bearing mice were intravenously injected with HSA (1 mg per mouse), and tumors were isolated after 2 hours and stained with anti-HSA immunoglobulin G to localize HSA in tumors.

mice 2 hours after injection using immunostaining with anti-HSA immunoglobulin G (Figure 7*B*). We found a strong staining of HSA in B16 tumors around the blood vessels, whereas only a very faint staining was present in C26 tumors. These results demonstrate that B16 tumors have high HSA uptake compared with the C26 tumors, and combined with the rapid and reversible binding of 15d-PGJ_2 to albumin found *in vitro*, this explains the effects of 15d-PGJ_2 in B16 tumors. Exogenous 15d-PGJ_2 can be an effective drug in tumor models, but its effectiveness *in vivo* is governed by an enhanced permeability and retention effect and local release from albumin.

Discussion

15d-PGJ_2 is an endogenous cellular growth modulator and has been shown to induce cytotoxic effects *in vitro* in different cancer cell types [28]. However, there is a clear lack of data showing its efficacy *in vivo* in animal tumor models. The present study demonstrates that 15d-PGJ_2 is able to inhibit the tumor progression effectively in a subcutaneous tumor model in mice. However, these effects were found to be dependent on its albumin-binding properties and on the characteristics of tumor vasculature, rather than on the sensitivity of tumor cells. 15d-PGJ_2 induced cell death *in vitro* in two different tumor cell types, namely, B16 melanoma and C26 colon carcinoma cells, through NF-κB– and caspase-dependent pathways. C26 cells seemed to be the most sensitive, but *in vivo* only B16 tumor growth was inhibited. We showed that 15d-PGJ_2 had a high binding affinity to albumin, and therefore, albumin most likely acts as a carrier for 15d-PGJ_2 in the circulation. Furthermore, we demonstrated that B16 tumors had larger blood vessel lumina compared with the C26 tumors and had a higher distribution of radiolabeled albumin. These data suggest that *in vivo* 15d-PGJ_2 may be highly effective in tumors with a vasculature that allows an efficient and high albumin uptake.

In the last decade, the cell death–inducing effect of 15d-PGJ_2 has been studied extensively in cultured cells of various cellular carcinomas such as breast, pancreatic, colon and gastric carcinomas, and B-cell lymphoma [11–15,29–31]. In these reports, the effects of 15d-PGJ_2 were shown to be mediated through PPARγ-dependent as well as PPARγ-independent pathways. In addition, the PPARγ-dependency

was irrespective of the type of cellular carcinoma because 15d-PGJ_2 inhibited the growth of different colon carcinoma cells through PPARγ-dependent or -independent pathways [15,32–34]. In the present study, we used two different carcinoma cell types to examine the effect of 15d-PGJ_2. However, there is no study showing the effect of 15d-PGJ_2 in these tumor cells or on any other tumor model. Although 15d-PGJ_2 is a PPARγ agonist, it exerted its cytotoxicity through PPARγ-independent pathways as shown by the lack of any effect of the irreversible PPARγ antagonist GW9662. Importantly, cell death in both cell types was found to be induced through the common PPARγ-independent mechanisms, namely, caspase- and NF-κB–dependent pathways, as demonstrated by the induction of proapoptotic enzymes caspase-3 and -7 and by the inhibition of the TNF-α–induced NF-κB activity in NF-κB–containing plasmid-transfected cells. 15d-PGJ_2 is a known negative regulator of NF-κB activity [35,36], and this was confirmed by our data. NF-κB plays an important role in the regulation of apoptosis by inhibiting or promoting apoptosis-regulating genes [37]. Therefore, the proapoptotic effect of 15d-PGJ_2 in B16 and C26 cells might be due to the inhibition of NF-κB activity as demonstrated in other cell types [38,39]. Of note, C26 cells were more sensitive to the 15d-PGJ_2 treatment than B16 cells as found repetitively in the present study.

Several studies have found that 15d-PGJ_2 loses its biologic activity *in vitro* in the presence of serum [17,18], which was also confirmed by us in this study. On the basis of the latter outcome, one may conclude that 15d-PGJ_2 would become inactive *in vivo* because a large amount of albumin is present in the circulation. However, our *in vivo* data showed that treatment with 15d-PGJ_2 substantially diminished the growth of subcutaneous B16 tumors in mice. In addition, the 15d-PGJ_2–treated tumors had higher damaged tumor tissue and disrupted vasculature. In line with our data, 15d-PGJ_2 has been shown to cause apoptosis in endothelial cells [40], which might be the reason for the disrupted vasculature in 15d-PGJ_2–treated mice. Conversely, no effect of 15d-PGJ_2 in C26 tumors was seen, which is in contrast to our *in vitro* studies. These data clearly indicate that 15d-PGJ_2 remained active after intravenous administration, but other factors govern the *in vivo* activity of 15d-PGJ_2.

Inactivation of 15d-PGJ_2 by serum proteins has been suggested as an important factor [17]. Albumin has a free –SH group in cysteine 34 [41] that may produce a stable covalent bond with the electrophilic cyclopentanone ring of 15d-PGJ_2 [7]. However, our gel filtration chromatography data revealed that the binding of 15d-PGJ_2 to albumin (HSA or mouse albumin) was reversible. Also, the incomplete blockade of the 15d-PGJ_2 effect by albumin in C26 cells *in vitro* (60% inhibition of the effect, see Figure 5*D*) at concentrations when nearly all 15d-PGJ_2 was bound to albumin suggests reversibility of the binding in C26 cells and may be due to the capacity of these cells to internalize the complex (see Figure 5*E*). So, covalent binding and inactivation of 15d-PGJ_2 through binding to –SH groups of albumin are unlikely; more likely, albumin serves as a reversible transport vehicle, transiently inactivating 15d-PGJ_2 and profoundly determining its body distribution.

Tumor vasculature is one of the most important factors regulating the accumulation of macromolecules (>40 kDa) such as albumin in tumors through a phenomenon referred to as enhanced permeability and retention [42]. Infiltration of macromolecules is regulated by tumor blood vessel density, blood vessel diameter and vascular permeability. Our γ-camera imaging and anti-HSA immunostaining data demonstrated that HSA distribution was much higher in B16 tumors compared with C26 tumors, which was correlated with a larger blood vessel lumen in B16 tumors than C26 tumors. Apparently, high blood vessel density does not enhance HSA uptake in these tumors because C26 tumors had significantly high blood vessel density but low HSA uptake compared with B16 tumors. Our data suggest that the antitumor effects of 15d-PGJ_2 in B16 tumors are related to the high HSA uptake in this tumor type, rather than to its sensitivity for 15d-PGJ_2. B16 tumors are more easily accessible for 15d-PGJ_2–albumin than C26 tumors. This might also be the reason that 15d-PGJ_2 has been found to display its therapeutic effects in many inflammatory diseases such as cystitis, acute pancreatitis, ischemia-reperfusion injury in gastric mucosa, brain, and kidneys [19,21–23,43,44] in animal models as the albumin permeability is enhanced during inflammation [45–48]. Because we showed that binding of 15d-PGJ_2 to albumin is reversible, 15d-PGJ_2 can be released from the albumin–15d-PGJ_2 complex after permeabilization into the diseased organ or tumor.

Moreover, no fatalities and toxicity to liver and kidneys were found after the multiple doses of 15d-PGJ_2 in both tumor models, which indicate that the applied doses were quite tolerable.

In conclusion, the present study shows that 15d-PGJ_2 can be an effective therapeutic agent for the treatment of cancer, but its effects are dependent on the tumor permeability of albumin that is determined by the tumor vasculature. This will greatly determine the rate of success of any study with 15d-PGJ_2, and it should therefore be taken into account before experimental or clinical studies with 15d-PGJ_2 or similar compounds. In addition, this study suggests that prevention of 15d-PGJ_2 binding to albumin using drug delivery strategies, such as incorporation into liposomes or conjugation to a protein carrier, might provide a novel strategy to improve its *in vivo* efficacy in tumors. 15d-PGJ_2 is a lipophilic compound and therefore can be incorporated into the lipid phase of liposomes. In addition, 15d-PGJ_2 has a carboxylic group at the terminal that is not important for its biologic activity but can be used for coupling to a protein carrier, which may result in an improved efficacy *in vivo*.

Acknowledgments

The authors thank Catharina Reker-Smit and Annemiek M. van Loenen-Weemaes for their excellent technical assistance. Authors also thank J.H. Pol and J. ter Veen from the Department of the Nuclear Medicine for the radiolabeling of albumin and helping in γ-camera imaging, respectively.

References

[1] Smith WL (1992). Prostanoid biosynthesis and mechanisms of action. *Am J Physiol* **263**, F181–F191.

[2] Kliewer SA, Lenhard JM, Willson TM, Patel I, Morris DC, and Lehmann JM (1995). A prostaglandin J_2 metabolite binds peroxisome proliferator–activated receptor γ and promotes adipocyte differentiation. *Cell* **83**, 813–819.

[3] Scher JU and Pillinger MH (2005). 15d-PGJ_2: the anti-inflammatory prostaglandin? *Clin Immunol* **114**, 100–109.

[4] Li L, Julien B, Grenard P, Teixeira-Clerc F, Mallat A, and Lotersztajn S (2004). Molecular mechanisms regulating the antifibrogenic protein heme-oxygenase-1 in human hepatic myofibroblasts. *J Hepatol* **41**, 407–413.

[5] Ferguson HE, Kulkarni A, Lehmann GM, Garcia-Bates TM, Thatcher TH, Huxlin KR, Phipps RP, and Sime PJ (2009). Electrophilic peroxisome proliferator activated receptor-{gamma} (PPAR{gamma}) ligands have potent anti-fibrotic effects in human lung fibroblasts. *Am J Respir Cell Mol Biol*. DOI: 10.1165 [Epub ahead of print 13 March].

[6] Li L, Tao J, Davaille J, Feral C, Mallat A, Rieusset J, Vidal H, and Lotersztajn S (2001). 15-Deoxy-Δ 12,14-prostaglandin J_2 induces apoptosis of human hepatic myofibroblasts. A pathway involving oxidative stress independently of peroxisome-proliferator–activated receptors. *J Biol Chem* **276**, 38152–38158.

[7] Uchida K and Shibata T (2008). 15-Deoxy-Δ(12,14)-prostaglandin J_2: an electrophilic trigger of cellular responses. *Chem Res Toxicol* **21**, 138–144.

[8] Bell-Parikh LC, Ide T, Lawson JA, McNamara P, Reilly M, and FitzGerald GA (2003). Biosynthesis of 15-deoxy-$\Delta^{12,14}$-PGJ_2 and the ligation of PPARγ. *J Clin Invest* **112**, 945–955.

[9] Staels B, Koenig W, Habib A, Merval R, Lebret M, Torra IP, Delerive P, Fadel A, Chinetti G, Fruchart JC, et al. (1998). Activation of human aortic smooth-muscle cells is inhibited by PPARα but not by PPARγ activators. *Nature* **393**, 790–793.

[10] Itoh K, Mochizuki M, Ishii Y, Ishii T, Shibata T, Kawamoto Y, Kelly V, Sekizawa K, Uchida K, and Yamamoto M (2004). Transcription factor Nrf2 regulates inflammation by mediating the effect of 15-deoxy-Δ(12,14)-prostaglandin J(2). *Mol Cell Biol* **24**, 36–45.

[11] Qiao L, Dai Y, Gu Q, Chan KW, Zou B, Ma J, Wang J, Lan HY, and Wong BC (2008). Down-regulation of X-linked inhibitor of apoptosis synergistically enhanced peroxisome proliferator–activated receptor γ ligand–induced growth inhibition in colon cancer. *Mol Cancer Ther* **7**, 2203–2211.

[12] Ray DM, Akbiyik F, and Phipps RP (2006). The peroxisome proliferator–activated receptor γ (PPARγ) ligands 15-deoxy-$\Delta^{12,14}$-prostaglandin J_2 and ciglitazone induce human B lymphocyte and B cell lymphoma apoptosis by PPARγ-independent mechanisms. *J Immunol* **177**, 5068–5076.

[13] Hashimoto K, Farrow BJ, and Evers BM (2004). Activation and role of MAP kinases in 15d-PGJ_2–induced apoptosis in the human pancreatic cancer cell line MIA PaCa-2. *Pancreas* **28**, 153–159.

[14] Li MY, Deng H, Zhao JM, Dai D, and Tan XY (2003). Peroxisome proliferator–activated receptor γ ligands inhibit cell growth and induce apoptosis in human liver cancer BEL-7402 cells. *World J Gastroenterol* **9**, 1683–1688.

[15] Shimada T, Kojima K, Yoshiura K, Hiraishi H, and Terano A (2002). Characteristics of the peroxisome proliferator activated receptor γ (PPARγ) ligand induced apoptosis in colon cancer cells. *Gut* **50**, 658–664.

[16] Fulzele SV, Chatterjee A, Shaik MS, Jackson T, Ichite N, and Singh M (2007). 15-Deoxy-$\Delta^{12,14}$-prostaglandin J_2 enhances docetaxel anti-tumor activity against A549 and H460 non–small-cell lung cancer cell lines and xenograft tumors. *Anticancer Drugs* **18**, 65–78.

[17] Person EC, Waite LL, Taylor RN, and Scanlan TS (2001). Albumin regulates induction of peroxisome proliferator–activated receptor-γ (PPARγ) by 15-deoxy-Δ(12-14)-prostaglandin J(2) *in vitro* and may be an important regulator of PPARγ function *in vivo*. *Endocrinology* **142**, 551–556.

[18] Hagens WI, Mattos A, Greupink R, de Jager-Krikken A, Reker-Smit C, van Loenen-Weemaes A, Gouw IA, Poelstra K, and Beljaars L (2007). Targeting 15d-prostaglandin J_2 to hepatic stellate cells: two options evaluated. *Pharm Res* **24**, 566–574.

[19] Hashimoto K, Ethridge RT, Saito H, Rajaraman S, and Evers BM (2003). The PPARγ ligand, 15d-PGJ_2, attenuates the severity of cerulein-induced acute pancreatitis. *Pancreas* **27**, 58–66.

[20] Zingarelli B, Hake PW, Mangeshkar P, O'Connor M, Burroughs TJ, Piraino G, Denenberg A, and Wong HR (2007). Diverse cardioprotective signaling mechanisms of peroxisome proliferator–activated receptor-γ ligands, 15-deoxy-$\Delta^{12,14}$-prostaglandin J_2 and ciglitazone, in reperfusion injury: role of nuclear factor-κB, heat shock factor 1, and Akt. *Shock* **28**, 554–563.

[21] Lin TN, Cheung WM, Wu JS, Chen JJ, Lin H, Chen JJ, Liou JY, Shyue SK, and Wu KK (2006). 15d-Prostaglandin J_2 protects brain from ischemia-reperfusion injury. *Arterioscler Thromb Vasc Biol* **26**, 481–487.

[22] Chatterjee PK, Patel NS, Cuzzocrea S, Brown PA, Stewart KN, Mota-Filipe H, Britti D, Eberhardt W, Pfeilschifter J, and Thiemermann C (2004). The cyclopentenone prostaglandin 15-deoxy-Δ(12,14)-prostaglandin J_2 ameliorates ischemic acute renal failure. *Cardiovasc Res* **61**, 630–643.

[23] Takagi T, Naito Y, Ichikawa H, Tomatsuri N, Katada K, Isozaki Y, Kuroda M, Kokura S, Yoshida N, and Yoshikawa T (2004). A PPAR-γ ligand, 15-deoxy-$\Delta^{12,14}$-prostaglandin J(2), inhibited gastric mucosal injury induced by ischemia-reperfusion in rats. *Redox Rep* **9**, 376–381.

[24] Cuzzocrea S, Pisano B, Dugo L, Ianaro A, Patel NS, Di PR, Genovese T, Chatterjee PK, Di RM, Caputi AP, et al. (2003). Rosiglitazone and 15-deoxy-$\Delta^{12,14}$-prostaglandin J_2, ligands of the peroxisome proliferator–activated receptor-γ (PPAR-γ), reduce ischaemia/reperfusion injury of the gut. *Br J Pharmacol* **140**, 366–376.

[25] Sengupta S, Eavarone D, Capila I, Zhao G, Watson N, Kiziltepe T, and Sasisekharan R (2005). Temporal targeting of tumour cells and neovasculature with a nanoscale delivery system. *Nature* **436**, 568–572.

[26] Satchi-Fainaro R, Puder M, Davies JW, Tran HT, Sampson DA, Greene AK, Corfas G, and Folkman J (2004). Targeting angiogenesis with a conjugate of HPMA copolymer and TNP-470. *Nat Med* **10**, 255–261.

[27] Mather SJ and Ward BG (1987). High efficiency iodination of monoclonal antibodies for radiotherapy. *J Nucl Med* **28**, 1034–1036.

[28] Ishihara S, Rumi MA, Okuyama T, and Kinoshita Y (2004). Effect of prostaglandins on the regulation of tumor growth. *Curr Med Chem Anticancer Agents* **4**, 379–387.

[29] Cekanova M, Yuan JS, Li X, Kim K, and Baek SJ (2008). Gene alterations by peroxisome proliferator–activated receptor γ agonists in human colorectal cancer cells. *Int J Oncol* **32**, 809–819.

[30] Kim EH, Na HK, and Surh YJ (2006). Upregulation of VEGF by 15-deoxy-$\Delta^{12,14}$-prostaglandin J_2 via heme oxygenase-1 and ERK1/2 signaling in MCF-7 cells. *Ann N Y Acad Sci* **1090**, 375–384.

[31] Ota K, Ito K, Suzuki T, Saito S, Tamura M, Hayashi S, Okamura K, Sasano H, and Yaegashi N (2006). Peroxisome proliferator–activated receptor γ and growth inhibition by its ligands in uterine endometrial carcinoma. *Clin Cancer Res* **12**, 4200–4208.

[32] Qiao L, Dai Y, Gu Q, Chan KW, Ma J, Lan HY, Zou B, Rocken C, Ebert MP, and Wong BC (2008). Loss of XIAP sensitizes colon cancer cells to PPARγ independent antitumor effects of troglitazone and 15-PGJ_2. *Cancer Lett* **268**, 260–271.

[33] Shen D, Deng C, and Zhang M (2007). Peroxisome proliferator–activated receptor γ agonists inhibit the proliferation and invasion of human colon cancer cells. *Postgrad Med J* **83**, 414–419.

[34] Chen ZY and Tseng CC (2005). 15-Deoxy-$\Delta^{12,14}$ prostaglandin J_2 up-regulates Kruppel-like factor 4 expression independently of peroxisome proliferator–activated receptor γ by activating the mitogen-activated protein kinase kinase/extracellular signal–regulated kinase signal transduction pathway in HT-29 colon cancer cells. *Mol Pharmacol* **68**, 1203–1213.

[35] Rossi A, Kapahi P, Natoli G, Takahashi T, Chen Y, Karin M, and Santoro MG (2000). Anti-inflammatory cyclopentenone prostaglandins are direct inhibitors of IκB kinase. *Nature* **403**, 103–108.

[36] Straus DS, Pascual G, Li M, Welch JS, Ricote M, Hsiang CH, Sengchanthalangsy LL, Ghosh G, and Glass CK (2000). 15-Deoxy-Δ 12,14-prostaglandin J_2 inhibits multiple steps in the NF-κ B signaling pathway. *Proc Natl Acad Sci USA* **97**, 4844–4849.

[37] Barkett M and Gilmore TD (1999). Control of apoptosis by Rel/NF-κB transcription factors. *Oncogene* **18**, 6910–6924.

[38] Castrillo A, Diaz-Guerra MJ, Hortelano S, Martin-Sanz P, and Bosca L (2000). Inhibition of IκB kinase and IκB phosphorylation by 15-deoxy-Δ(12,14)-prostaglandin J(2) in activated murine macrophages. *Mol Cell Biol* **20**, 1692–1698.

[39] Piva R, Gianferretti P, Ciucci A, Taulli R, Belardo G, and Santoro MG (2005). 15-Deoxy-Δ 12,14-prostaglandin J_2 induces apoptosis in human malignant B cells: an effect associated with inhibition of NF-κ B activity and down-regulation of antiapoptotic proteins. *Blood* **105**, 1750–1758.

[40] Kaplan J, Cook JA, O'Connor M, and Zingarelli B (2007). Peroxisome proliferator–activated receptor γ is required for the inhibitory effect of ciglitazone but not 15-deoxy-Δ 12,14-prostaglandin J_2 on the NFκB pathway in human endothelial cells. *Shock* **28**, 722–726.

[41] Kratz F, Warnecke A, Scheuermann K, Stockmar C, Schwab J, Lazar P, Druckes P, Esser N, Drevs J, Rognan D, et al. (2002). Probing the cysteine-34 position of endogenous serum albumin with thiol-binding doxorubicin derivatives. Improved efficacy of an acid-sensitive doxorubicin derivative with specific albumin-binding properties compared to that of the parent compound. *J Med Chem* **45**, 5523–5533.

[42] Jang SH, Wientjes MG, Lu D, and Au JL (2003). Drug delivery and transport to solid tumors. *Pharm Res* **20**, 1337–1350.

[43] Masuda H, Chancellor MB, Kihara K, and Yoshimura N (2006). 15-Deoxy-$\Delta^{12,14}$-prostaglandin J_2 attenuates development of cyclophosphamide-induced cystitis in rats. *Urology* **67**, 435–439.

[44] Abdelrahman M, Collin M, and Thiemermann C (2004). The peroxisome proliferator–activated receptor-γ ligand 15-deoxy$\Delta^{12,14}$ prostaglandin J_2 reduces the organ injury in hemorrhagic shock. *Shock* **22**, 555–561.

[45] Mochizuki M, Ishii Y, Itoh K, Iizuka T, Morishima Y, Kimura T, Kiwamoto T, Matsuno Y, Hegab AE, Nomura A, et al. (2005). Role of 15-deoxy Δ(12,14) prostaglandin J_2 and Nrf2 pathways in protection against acute lung injury. *Am J Respir Crit Care Med* **171**, 1260–1266.

[46] Muller MW, McNeil PL, Buchler P, Ceyhan GO, Wolf-Hieber E, Adler G, Beger HG, Buchler MW, and Friess H (2007). Acinar cell membrane disruption is an early event in experimental acute pancreatitis in rats. *Pancreas* **35**, e30–e40.

[47] Uchida K, Mishima S, Ohta S, and Yukioka T (2007). Inhibition of inducible nitric oxide synthase ameliorates lung injury in rats after gut ischemia-reperfusion. *J Trauma* **63**, 603–607.

[48] McCarthy ET, Sharma R, Sharma M, Li JZ, Ge XL, Dileepan KN, and Savin VJ (1998). TNF-α increases albumin permeability of isolated rat glomeruli through the generation of superoxide. *J Am Soc Nephrol* **9**, 433–438.